CHAPTER 4

Structural and mesomorphic properties of a few hockey stick-shaped compounds with a lateral methyl group showing nematic, synclinic and anticlinic smectic C phases

4.1. Introduction

In recent years, the "hockey- stick" shaped liquid crystals with a shape intermediate between the traditional rod-like molecules and the conventional bent-cores, have emerged as a field of considerable interest in soft matter research. Some of these compounds are of additional importance due the occurrence of two polymorphic tilted smectic phases – the synclinic smectic *C* (Sm–C_s) and the anticlinic smectic *C* (Sm-C_a) phases. In the Sm-C_s phase, the direction of the tilt is the same in adjacent smectic layers, whereas it alternates between the layers of the Sm-C_a phase. This dimorphism is only rarely observed for non-chiral compounds. In previous works, for a homologous series of 4-(3-*n*-decycloxy phenylimino-methyl)phenyl 4-*n*-alkyloxybenzoate compounds, comprising a *meta*-alkyloxy substituted three-ring core with a COO and a CH=N linking group between the phenyl rings, the occurrence of Sm-*A* phase, Sm-C_s and Sm-C_a phases have been observed depending upon the length of the terminal chains [1–4]. From NMR investigations on these compounds it was confirmed that the Sm-C_s–Sm-C_a phase transition is accompanied by a conformational change in the molecular part containing the 3-alkyloxyphenyl fragment [1]. This conformational change is associated with a change in the shape of the molecules from a more rod-like one in the Sm-C_s

phase to a hockey stick like shape in the Sm-C_a phase and leads to a different packing of the molecules within the layers of the Sm-C_a phase.

The enlargement of the mesogenic aromatic core of the three-ring compounds by insertion of a carbon–carbon double bond results in esters of the cinnamic acid, which again exhibits Sm-*A*–Sm-C_s–Sm-C_a mesomorphism, however at a little higher temperature [5]. Interestingly, the dielectric anisotropy of these compounds changes from positive to negative values in the Sm-C_a phase, which could be related to the bent hockey-stick shape of the molecules in the Sm-C_a phase [1, 4]. Thus, it is of great interest to see whether any other modifications in the chemical structure of these hockey-stick shaped mesogens lead to new materials exhibiting interesting mesogenic properties or phase sequences.

In this chapter, study on the structural and mesomorphic behavior of five members of a homologous series of laterally methyl substituted hockey stick-shaped mesogenic 4-(3-*n*-alkyloxy-2-methyl-phenyliminomethyl)phenyl 4-*n*-alkyloxycinnamates from polarizing optical microscopy, X-ray diffraction, NMR, optical birefringence, dielectric and electro-optical methods has been reported [6]. The lateral methyl group is introduced in the obtuse angle between the *meta*-alkyloxy-chain attached to the terminal phenyl ring and the azomethine connecting group. The phase transition behavior of the compounds **1-5** has been listed in table 4.1. The 4-(3-*n*-alkyloxy-2-methyl-phenyliminomethyl)phenyl 4-*n*-alkyloxycinnamates (compounds **1-5**) exhibit a nematic phase in combination with an anticlinic Sm-*C* phase or in the *I*–*N*–Sm-C_s–Sm-C_a phase sequence. It may be mentioned that the Sm-C_a phase is relatively seldom, and the sequence Sm-C_s–Sm-C_a is also rare in case of mesogens having no asymmetric carbon atom except the case wherein the terminal chain is a branched chain (swallow tailed) [7, 8]. The occurrence of a nematic phase above smectic phases is pleasant because there is a better chance to orient the smectic phases. The phase transition temperatures were determined using polarizing optical microscopy, differential scanning

calorimetry and optical transmission measurements. This combination is helpful because the Sm-C_s–Sm-C_a transition exhibits only very low enthalpy values. Furthermore, this transition is clearly characterized by strong turbulences in the schlieren texture, which can persist over a temperature range of some degrees before absolutely coming to an end.

4.2. Materials

The mesophase behavior, transition temperatures and transition enthalpies of the compounds **1**–**5** are summarized in table 4.1. To allow a comparison between the two measuring methods, calorimetric data are given in the first line together with the enthalpy values in brackets. In the next line, temperatures obtained from optical transmission measurements have been listed in which the Sm-C_s–Sm-C_a transition is very prominent. The structural formula, as shown in table 4.1 includes the carbon positions required for assignment of the 1D NMR spectra.

Table 4.1. Molecular structure, transition temperatures (°C) and associated transition enthalpies (kJ mol^{-1}) for the 4-(3-*n*-alkyloxy-2-methyl-phenyliminomethyl)phenyl 4-*n*-alkyloxycinnamates. [a]

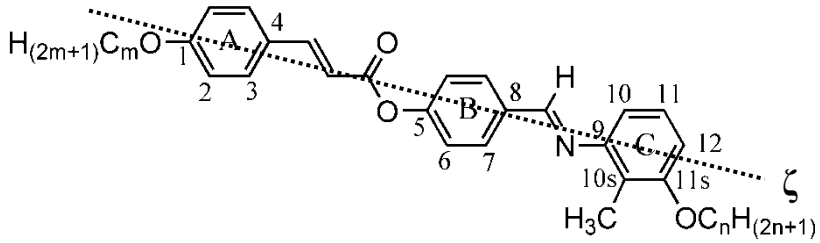

Compound	*m*	*n*	Cr		Sm-C_a		Sm-C_s		*N*		*I*
1	8	8	•	58.2[a] [47.4] 59.1	•		-	100.8 [1.8] 99.7	•	110.8 [0.49] 109.6	•
2	8	10	•	70.2 [28.9] 70.5	•		-	99.9 [1.5] 97.2	•	108.6 [0.48] 107.5	•
3	10	8	•	67.5 [31.3] 65.8	•	[b] 105.4	•	107.0 [2.0] 106.1	•	112.8 [0.23] 110.6	•
4	10	10	•	66.9 [38.2] 67.5	•	104 [0.03] 103.1	•	107.2 [2.6] 107.2	•	112 [0.98] 111.8	•
5	12	10	•	73.1 [68.7] 74.6	•	107.2 [0.15] 103.6	•	109.5 [c] 109.7	•	111.0 [5.8][c] 110.1	•

Notes:

[a] Transition temperatures: calorimetrically determined values (onset, on heating) (first line) with their transition enthalpies in brackets (second line) and those from the optical transmission measurements (third line).

[b] Phase transitions not observed by DSC.

[c] Phase transitions Sm-C_s–*N*–*I* not sufficiently resolved in the DSC curves.

•: Represents the corresponding phases are present; —: represents the absence of the phase.

4.3. Texture observation

The compounds **1**–**5** exhibit a nematic (*N*) phase which preferably shows homeotropic orientation. The clearing temperatures are near to 110 °C and surprisingly, they are about 10 K higher than that of corresponding compounds without lateral methyl group [5]. This effect is remarkable because small lateral alkyl groups attached to rod-like molecules generally decrease the mesophase stability. The finding is in agreement with results for other hockey-stick shaped compounds reported by Wu *et al.* [9, 10].

Upon cooling the nematic phase of the compounds **1** and **2**, a schlieren texture of a Sm-C_a phase appears. It shows disclination points with two brushes in addition to those with four brushes. This is evidence for an anticlinic arrangement of adjacent layers. It is in agreement with the symmetric diffraction pattern found by X-ray measurements (section 4.5) and allows to classify the phase as Sm-C_a.

A schlieren texture or a broken fan-shaped texture typical for synclinic Sm-C_s phases appears on cooling the nematic phases of the compounds **3**–**5** [figures 4.1(a) and (b)]. The transition into the low temperature Sm-C_a phase is accompanied by a clear change of the optical textures. The schlieren texture of the Sm-C_s phase differs strongly from that of the Sm-C_a phase [figure 4.1(c)]. Moreover, near the Sm-C_s–Sm-C_a transition the schlieren texture strongly fluctuates, which is a characteristic behavior at synclinic–anticlinic transitions. The fluctuations appear in a certain temperature range, and in some cases it is difficult to decide whether the transition is really finished. The reason is that the reorientation of the molecular tilt can proceed step by step in every second layer [2]. The broken fan-shaped texture of the Sm-C_s phase transforms by cooling into the Sm-C_a modification with a fan-shaped texture with irregular stripes across the fans [figure 4.1(d)]. The birefringence decreases as indicated by the change in the interference colors.

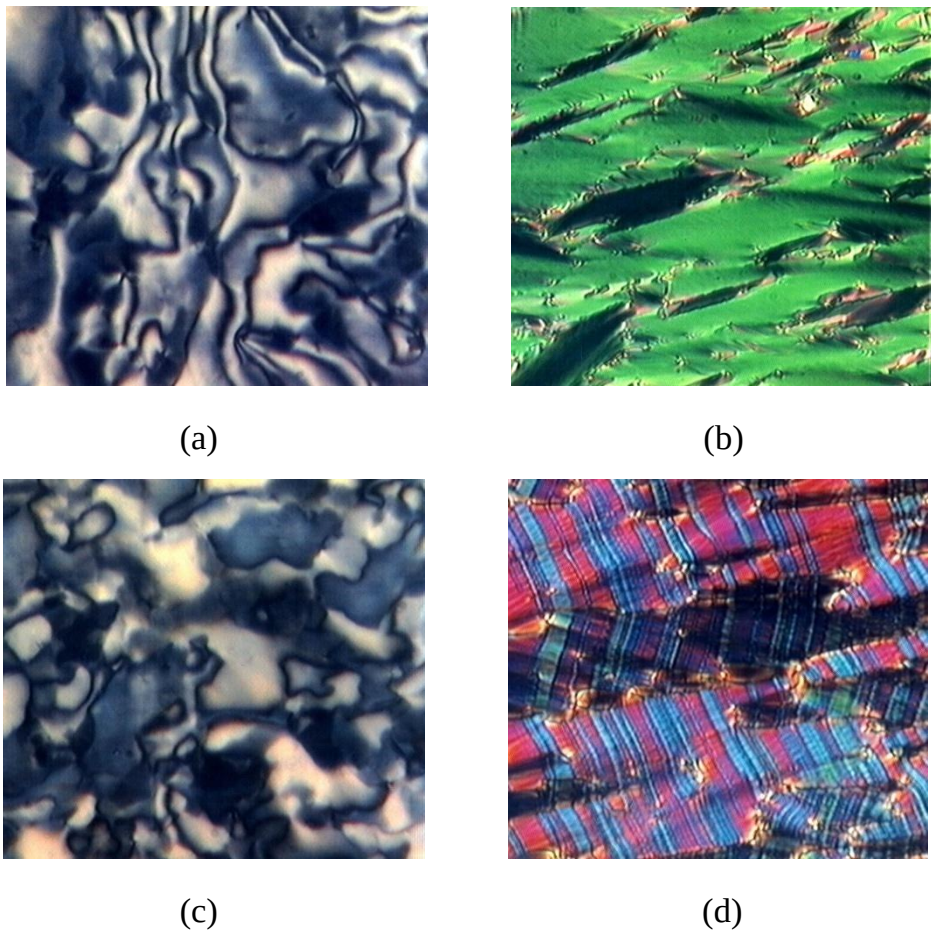

Figure 4.1. Compound **5**: (a) schlieren texture of the Sm-C_s phase, (b) broken fan-shaped texture of the Sm-C_s phase, (c) schlieren texture of the Sm-C_a phase, (d) fan-shaped texture of the Sm-C_a phase with irregular stripes: (a) and (b): 108 °C, (c) and (d): 100 °C.

4.4. Optical transmission study

An optical transmission method was used for the identification of different liquid crystalline phases in these compounds along with texture study, X-ray and DSC measurements. It was found that this method is an excellent tool for the determination of the phase transition temperatures, particularly for hockey stick compounds [4, 11]. The three phase transitions, *I*–*N*, *N*–Sm-C_a and Sm-C_s–Sm-C_a, of these compounds were clearly identified from the sharp change of the transmitted intensity values or change in the slope of the temperature dependent intensity curve. Since the Sm-C_s–Sm-C_a phase transition temperatures were not or only hardly detectable by DSC

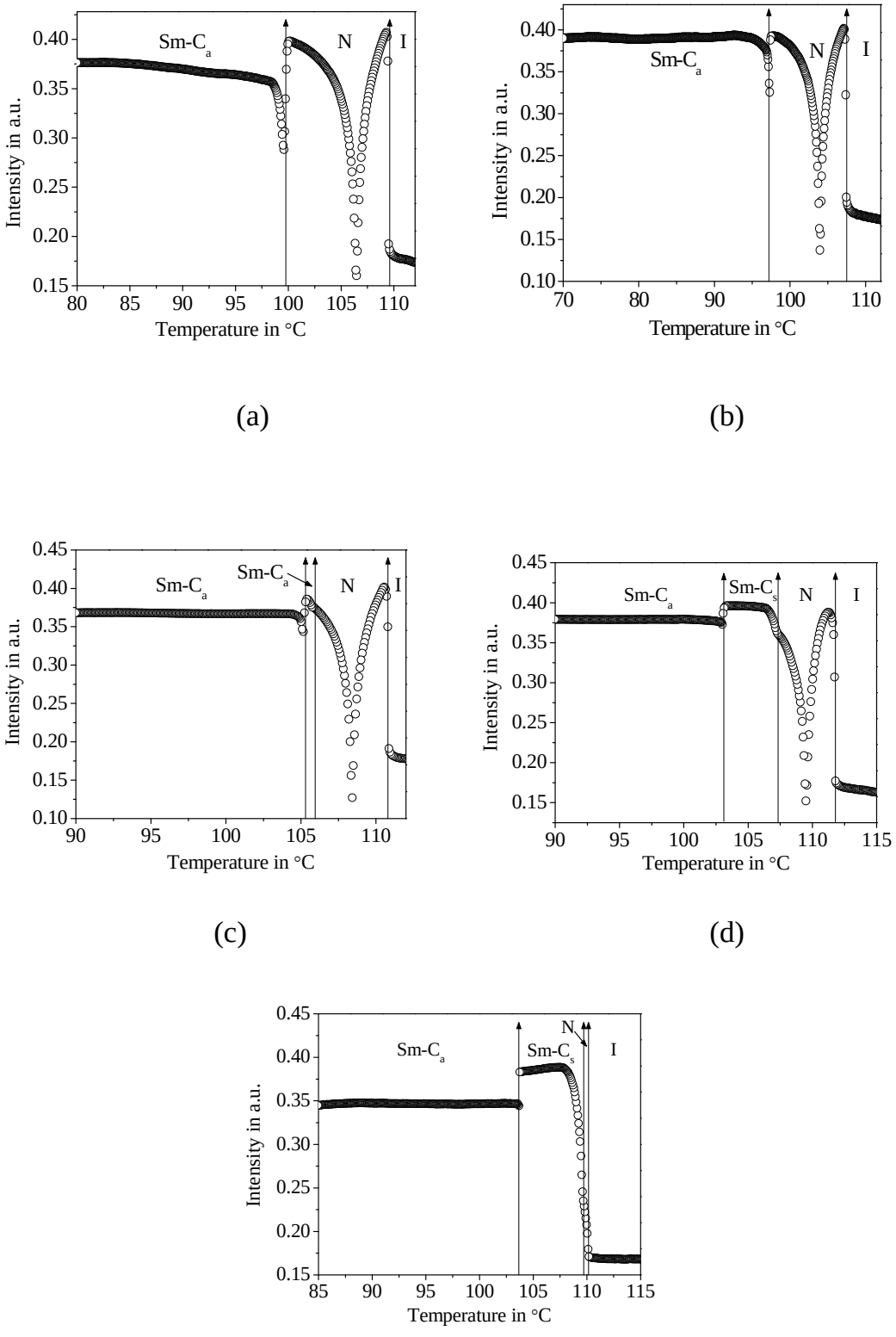

Figure 4.2. Transmitted intensity as a function of temperature during cooling of compounds (a) **1**, (b) **2**, (c) **3**, (d) **4** and (e) **5**.

measurements in some of these compounds due to their very small transition enthalpies, the optical transmission method proved to be very helpful in clearly pinpointing this transition. Figure 4.2 shows the temperature dependence of the optical intensity for the compounds **1**–**5.** From the transmitted intensity curve it can be concluded that compounds **1** and **2** have a *N* and a Sm-C_a phase only. On the other hand compounds **3**–**5** exhibit an *N*–Sm-C_s–Sm-C_a phase sequence. For compounds **3** and **4** the *N*, Sm-C_s and Sm-C_a phases exist in a sufficiently broad range to make physical measurements possible. It is to be noted that the intensity of the transmitted laser light depends upon the phase difference, $\Delta\varphi = \frac{2\pi}{\lambda}\Delta n d$, where Δn is the birefringence of the sample and *d* represents the cell thickness. Due to the oscillatory nature of $\Delta\varphi$, for a large change in the birefringence of the medium within the *N* phase, one minimum was observed for each sample except compound **5**.

4.5. X-ray investigations

X-ray diffraction measurements on surface-aligned samples of compounds **1** [figures 4.3(a) and 4.3(b)] and **2** clearly show the patterns of the high-temperature *N* phase (diffuse halos in the wide and in the small angle region, the high intensity of the inner halo indicating the existence of cybotactic groups of the smectic type) and that of the smectic phase at lower temperatures (very strong first and very weak second order layer reflections on the meridian of the pattern along with diffuse halos in the wide angle region). The layer spacing of compound **1** (**2**) decreases from 34.2 (37.4) Å at 99 (97) °C to 32.8 (36.5) Å at 70 (70) °C, respectively, while the tilt angle estimated from the positions of the maxima for the outer diffuse scattering increases from 22 (20)° to 29 (29)° in the same temperature interval. The azimuthal (χ-) distribution of the wide angle scattering around the trace of the primary beam shows four maxima for both compounds. The two maxima above the equator have equal intensities within experimental error indicating the co-existence of equal numbers of molecules with opposite tilt. (The part of the

pattern below the equator is shadowed by the heating stage.) This may arise from equally distributed domains of opposite tilt in the Sm-C_s phase or from an anticlinic tilt of molecules in adjacent layers, as found in the Sm-C_a phase.

Analogous X-ray investigations on compound **4** confirm the presence of three liquid crystalline phases. The pattern at 108 °C [figure 4.3(c)] shows diffuse scattering in both the inner and outer diffraction range with comparatively strong maxima on the equator (inner scattering) and on the meridian of the pattern (outer scattering), respectively, which is the typical pattern of a *N* phase showing cybotactic groups as in case of compounds **1** and **2**, but this time the nematic director is oriented on the average parallel to the aligning surface. At about 107 °C, the pattern changes, the small angle and wide angle diffraction maxima move to completely different positions and indicate that now the smectic layers are parallel to the glass plate. The maxima of the two outer diffraction arcs are rotated out off the equator by about 17° in the same sense of rotation indicating a structure with synclinically tilted molecules – the Sm-C_s phase [figure 4.3(d)]. At about 104°C, the X-ray pattern changes once more, now exhibiting broader halos for the outer diffuse scattering centered about the equator [figure 4.3(e)] closely resembling those in the patterns of the Sm-*C* phases of compounds **1** and **2**. The χ-distribution of their intensity was fitted by four Gaussian curves, the positions of the four maxima yielding a tilt angle of about 23°. The tilt slightly increases with decreasing temperature [figure 4.4(a)]. The statistical uncertainty for the determination of the tilt angles in one experimental setting is in the range of ±1° and the experimental error for the absolute value of the tilt due to the shadowing of the pattern is expected to be somewhat larger. As stated above, the X-ray diffraction measurements cannot distinguish between a rotationally disordered synclinic structure and an anticlinic molecular packing. However, considering the results of the other experiments, it can be safely concluded that the low-temperature phase is Sm-C_a. In accordance with the temperature dependence of the molecular tilt, the layer spacing decreases sharply from

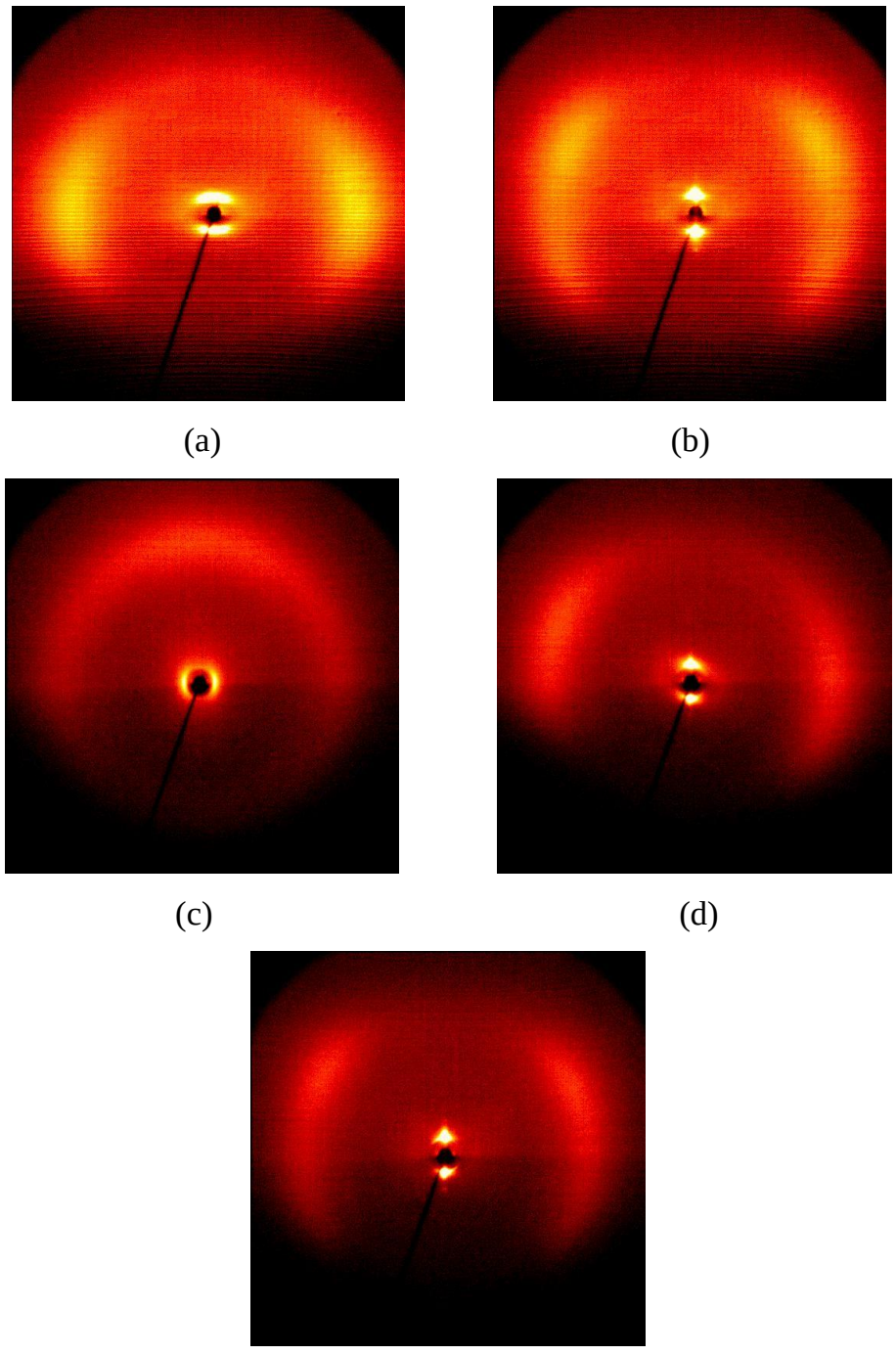

(a) (b)

(c) (d)

(e)

Figure 4.3. 2D X-ray diffraction patterns of surface-aligned samples of compounds **1** and **4** on cooling, meridian of the pattern normal to the aligning surface; compound **1**: (a) *N* phase at 102 °C, nematic director parallel to the meridian, (b) Sm-C_a phase at 95 °C, layers parallel to the aligning surface; compound **4**: (c) *N* phase at 108 °C, nematic director parallel to the aligning surface (d) Sm-C_s phase at 106 °C with a majority of domains showing the same tilt direction, layers parallel to the aligning surface, (e) Sm-C_a phase at 80 °C, layers parallel to the aligning surface.

37.6 Å at the *N*–Sm-C_s transition to 36.6 Å at the transition to Sm-C_a and then only slightly decreases to 36.0 Å at 80 °C [figure 4.4(b)], which means it remains more or less constant throughout the Sm-C_a phase.

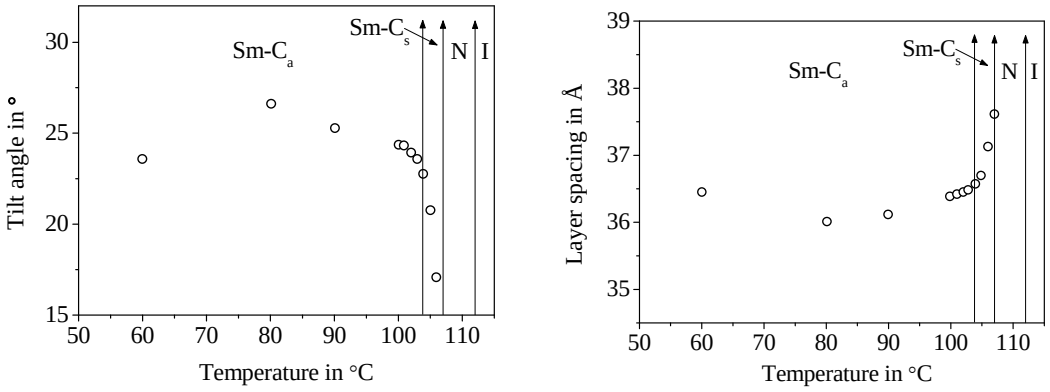

(a) (b)

Figure 4.4. Temperature dependence of (a) average tilt of the molecules with respect to the layer normal and (b) layer spacing on cooling as derived from the 2D X-ray patterns of compound **4**.

4.6. NMR investigations

^{13}C-NMR investigations have been performed on a few selected hockey stick-shaped compounds (compounds **3** and **4**) to obtain knowledge of the molecular ordering in the mesophases. The proton decoupled ^{13}C NMR spectra in the isotropic phase as well as at different temperatures in the *N*, Sm-C_s and Sm-C_a phases for compound **4** are shown in figure 4.5. The acquisition of all the spectra was carried out during cooling from the isotropic phase. The assignment of the lines in the isotropic spectrum rests upon the increment system. The assignment of the lines in the mesophases was made on the basis of both chemical shift anisotropies and also observing the trends of variation of the signals with temperature. Moreover, a comparison of the spectra with those of similar compounds reported earlier [1], also has provided additional support.

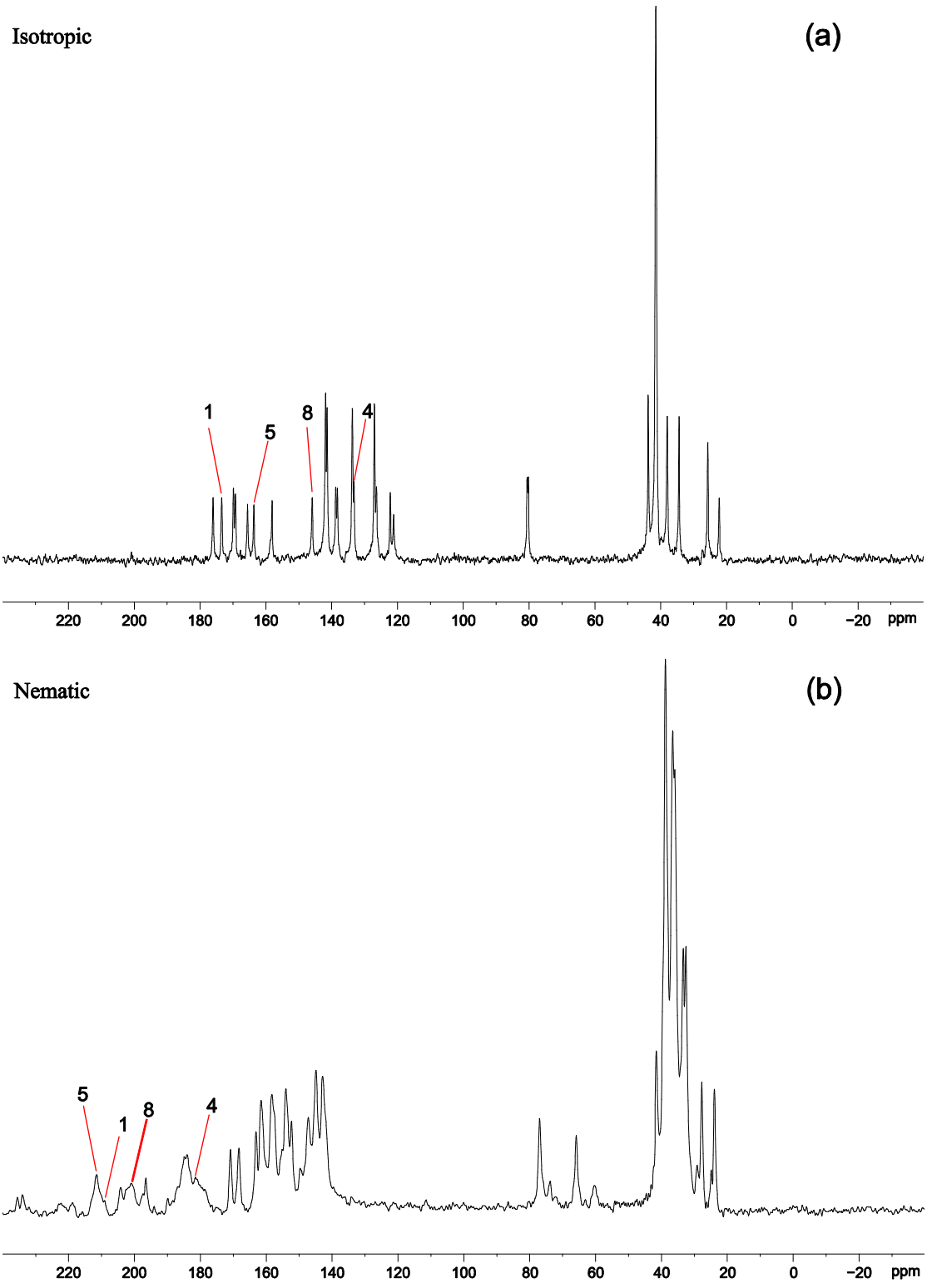

Figure 4.5. Proton decoupled ^{13}C NMR spectra (1D) of compound **4**: (a) *I* phase at 116.5 °C, (b) *N* phase at 111.5 °C.

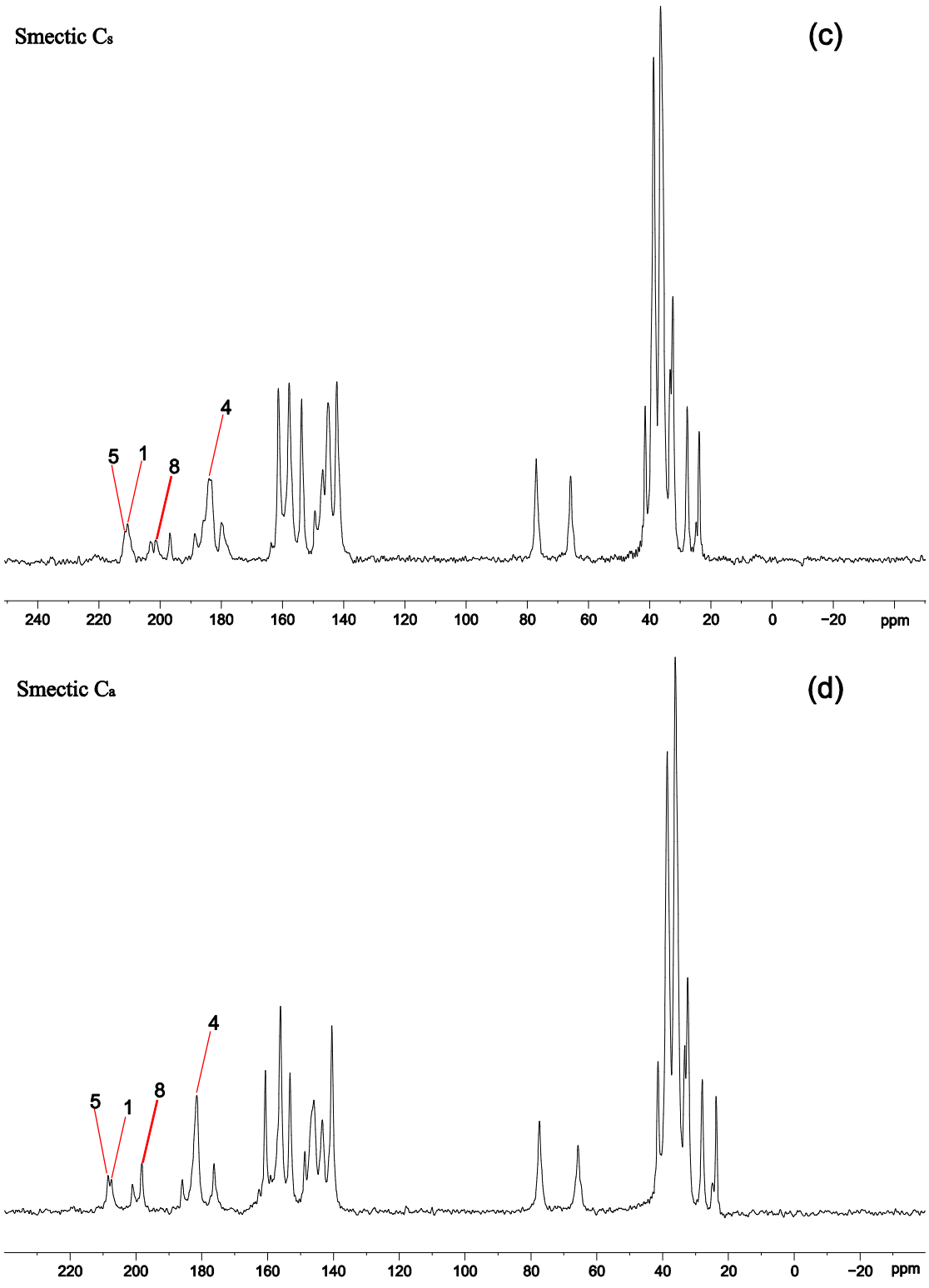

Figure 4.5. (cont'd). Proton decoupled ^{13}C NMR spectra (1D) of compound **4**: (c) Sm-C_s phase at 107.5 °C and (d) Sm-C_a phase at 90.5 °C.

4.7. Optical birefringence measurements

Birefringence measurements were carried out on compounds **1**–**5**, the temperature dependence of which has been shown in figures 4.6(a)–(e). Upon cooling, a significant increase of birefringence was observed within the *N* phase which is due to the increase in nematic order. For all the samples studied, the birefringence value was found to decrease at the Sm-C_s–Sm-C_a phase transition and remained more or less constant throughout the Sm-C_a phase. Such lowering of birefringence has also been observed from the color change of the optical texture during the phase transition.

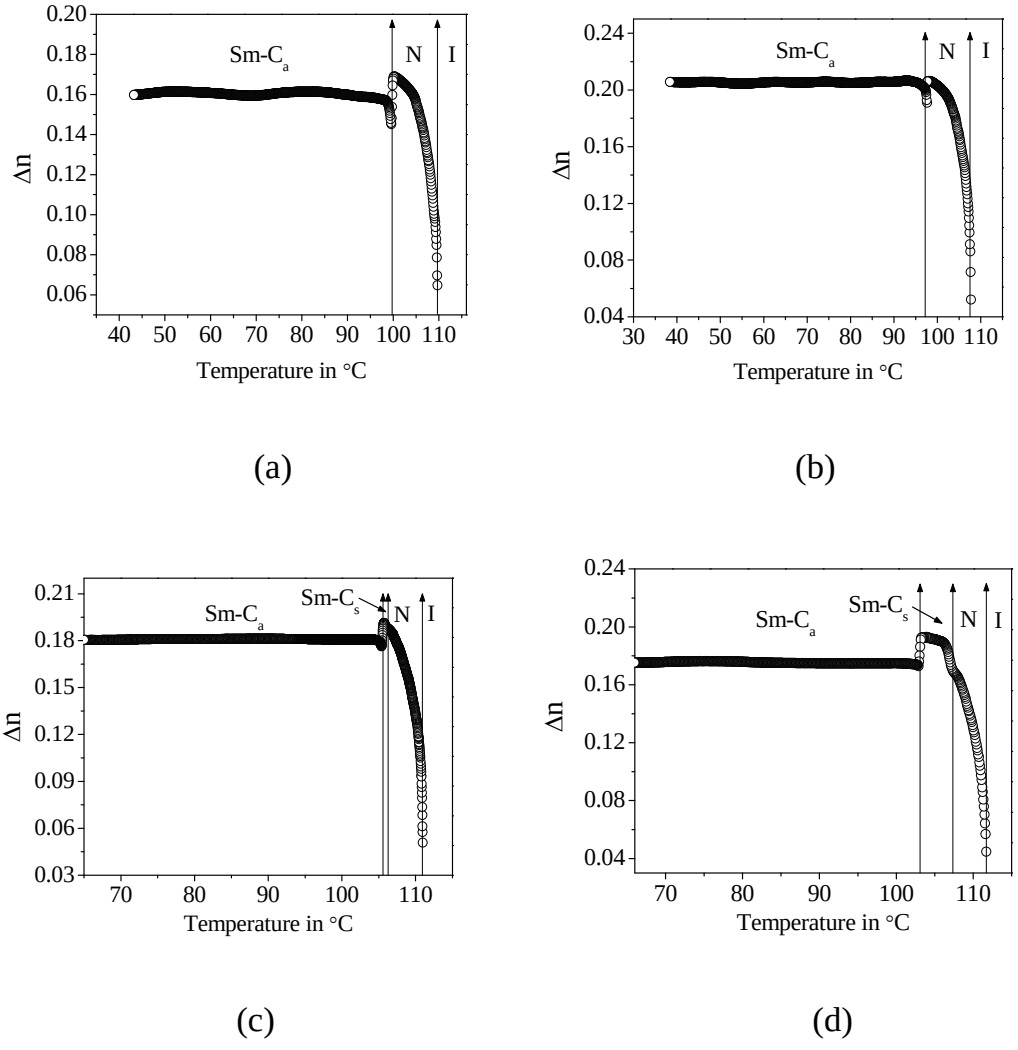

Figure 4.6. Temperature dependence of birefringence for the compounds (a) **1**, (b) **2**, (c) **3**, (d) **4**.

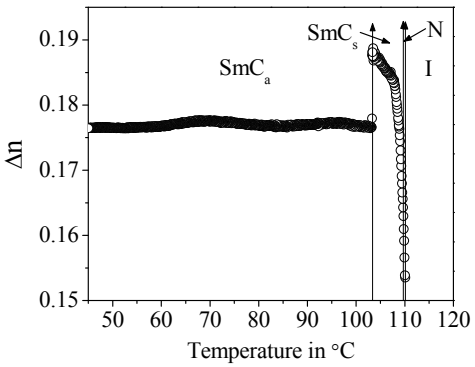

(e)

Figure 4.6. (cont'd). Temperature dependence of birefringence for the compound (e) **5**.

4.8. Orientational order parameter

The optical birefringence, Δn, obtained from the measured transmitted intensity data of the homogeneously aligned cell [12, 13] of thickness 5.1 μm was utilized to determine the temperature variation of the orientational order parameter in the liquid crystalline phases of these compounds. The order parameter is defined as $\langle P_2 \rangle = \Delta n/\Delta n_0$, where Δn_0 is the birefringence in the completely ordered state and was obtained from the temperature dependence of Δn, which can be approximated well for liquid crystals by [14]

$$\Delta n = \Delta n_0 \left(1 - \frac{T}{T^*}\right)^{\beta} \tag{4.1}$$

where Δn_0, T^* and β are adjustable parameters. T^* is about 1–2 K above the clearing temperature. The exponent β depends on the molecular structure and its value is close to 0.2. This procedure is correct only for oriented phases of single axis system. Therefore, equation (4.1) has been fitted for the compounds **1**–**4** by taking the values of Δn only for the *N* phase. As an attempt, equation (4.1) was applied for the Sm-C_s phase of compound **5**.

In table 4.2, the Δn values at a temperature 5 K below the Sm-C_s–Sm-C_a phase transition for all the five compounds along with the extrapolated

birefringence at the absolute zero temperature (Δn_0) has been represented. It is evident that for a fixed value of the chain length (n = 10), Δn decreases with increasing chain length m. Again, if m is kept constant (m = 10), Δn decreases with increasing chain length (n = 8–10). A similar behavior is also observed if one considers the extrapolated birefringence at the absolute zero temperature, Δn_0.

Table 4.2. Optical birefringence (Δn) in the Sm-C_a phase at a temperature 5 K below the Sm-C_s–Sm-C_a phase transition for all the five compounds and calculated values of Δn_0 and β (m, n: chain lengths as stated in table 4.1).

Compound (m, n)	**Δn**	**Δn_0**	**β**
1 (8, 8)	0.1589	0.318	0.162
2 (8, 10)	0.1941	0.403	0.172
3 (10, 8)	0.1912	0.371	0.153
4 (10, 10)	0.1827	0.344	0.150
5 (12, 10)	0.1867	0.380	0.145

The data presented in table 4.2 were used to calculate the order parameter $<P_2>$. This procedure was extended to the Sm-C phases in order to observe special orientation effects of the molecules during the formation of the different SmC modifications. The temperature dependence of $<P_2>$ is shown in figures 4.7(a)–(e). The experimental order parameter in the N and Sm-C_s phases increases with decreasing temperature. For compounds **3**, **4** and **5**, a drop is observed in the order parameter values at the Sm-C_s–Sm-C_a phase boundary. This may be due to the fact that the molecular long axes in the Sm-C_s phase of the surface aligned bulk sample are oriented parallel to the aligning surface and the layers are tilted with respect to the surface. Therefore a normal temperature dependence of the order parameter is observed in the Sm-C_s phase. However,

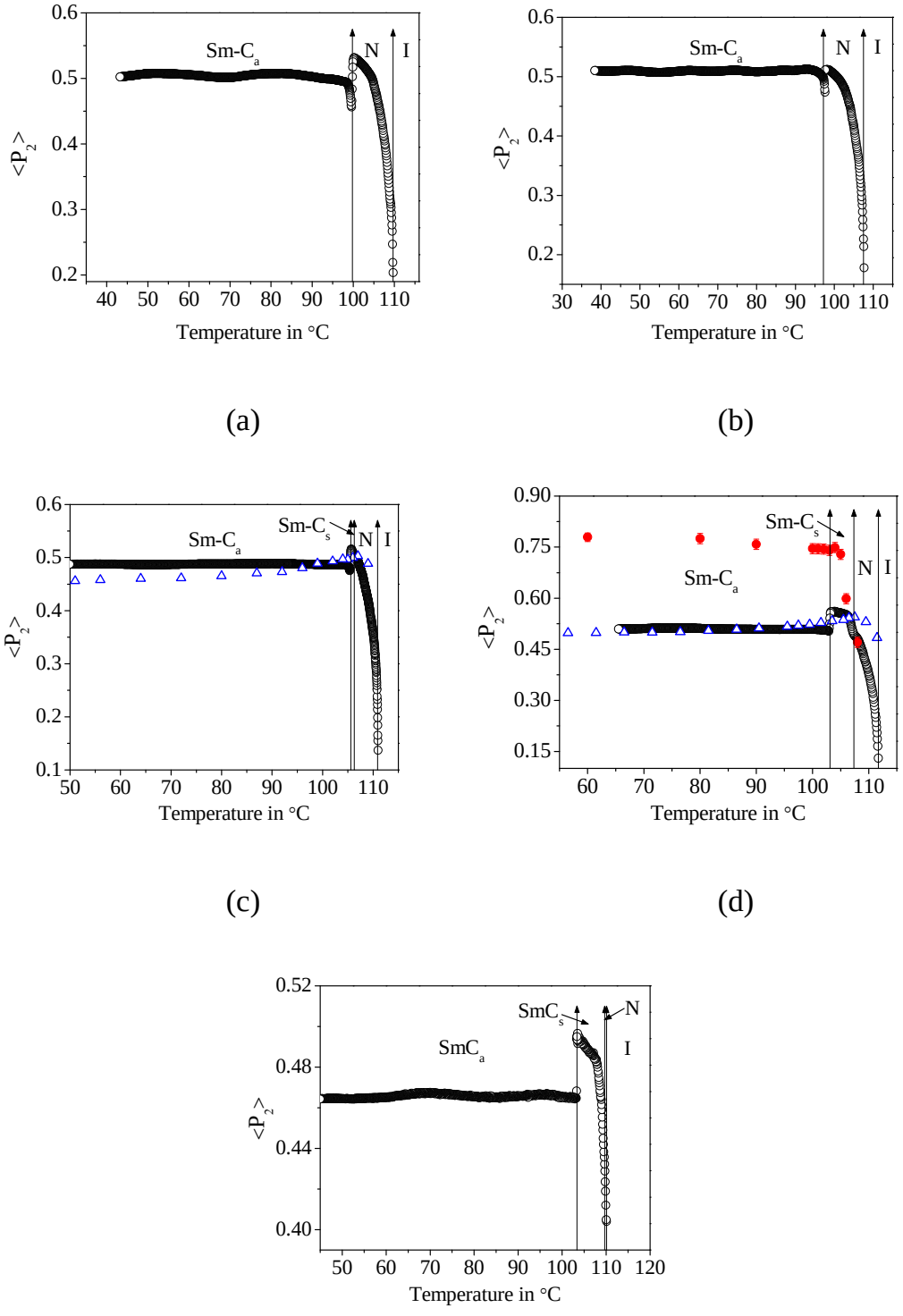

Figure 4.7. Temperature variation of $<P_2>$ for compounds (a) **1**, (b) **2**, (c) **3**, (d) **4** and (e) **5** (open circles show $<P_2>$ from birefringence measurements, closed ones in (d) show $<P_2>$ calculated from X-ray patterns and triangles in (c) and (d) show $<P_2>$ obtained from NMR measurements).

since the transition to the Sm-C_a phase in these compounds leads to an effective reorientation of the molecules to form an anticlinic arrangement, the molecules in this phase are now tilted with respect to the surface. This tilt of the molecules in the Sm-C_a phase causes a drop in the parallel component of the polarisability, i.e., along the molecular long axis, thereby reducing the polarisability anisotropy and hence, the birefringence of the material. Within the Sm-C_a phase the birefringence and hence, the order parameter $<P_2>$ remain constant.

The orientational distribution function $f(\beta)$ and hence the orientational order parameter $<P_2>$ of compound **4** have been determined from X-ray intensity data using the method suggested by Bhattacharya *et al.* [15]. For this purpose, a χ– scan (i.e., X-ray intensity I (χ) *vs.* azimuthal angle (χ) curve) of the outer diffraction arc for χ = -15 to χ = 335° (omitting the trace of the beam stop) was first performed for the patterns of the Sm-*C* phases and for that of the isotropic liquid. Then, the intensity data were calibrated by those of the isotropic liquid to correct them for influences of the experimental setting using $I_{rel} = I(80\ °C) / I(115\ °C$, isotropic liquid) assuming an isotropic χ– distribution of the outer diffuse scattering for the sample in the isotropic liquid [figure 4.8(a)]. This intensity distribution $I_{rel}(\chi)$ was then utilized to determine the orientational distribution function $f(\beta)$ and the order parameter $<P_2>$. From the values of $I(\chi)$, the distribution function $f(\beta)$ and hence the order parameter ($<P_2>$) have been calculated following Leadbetter's expression [16]. For determining the experimental $f(\beta)$ values and the order parameter $<P_2>$, the azimuthal distribution of the X-ray intensities $I(\chi)$ in one quadrant (e.g., from χ = 0° to χ = 90°) is sufficient. In the present case, due to the shadowing of the pattern by the heating stage the average values of $I(\chi)$ to calculate $f(\beta)$ and hence $<P_2>$, have been determined from the non-shadowed upper quadrants, i.e., from χ = 90° to χ = 270° only. The temperature variation of $<P_2>$ for compound **4** from the X-ray diffraction measurements has been shown in figure 4.7(d).

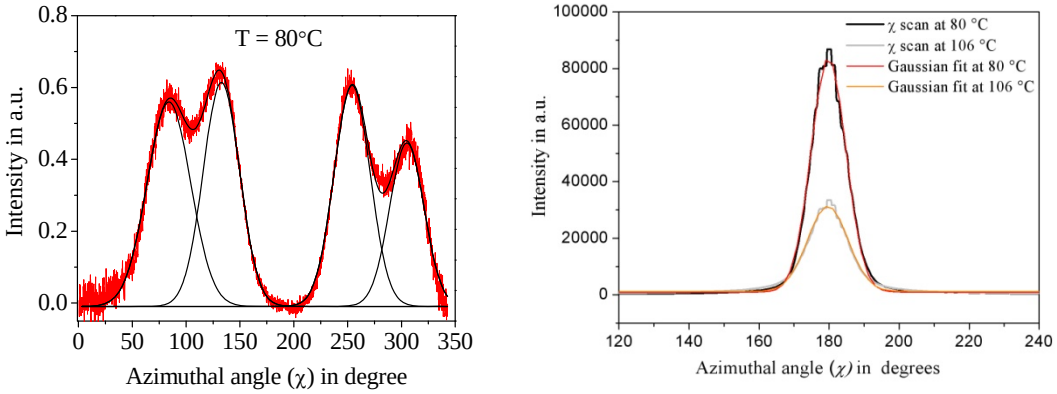

(a) (b)

Figure 4.8. χ scans of the 2D X-ray patterns for compound **4:** (a) outer diffuse scattering at 80 °C with Gaussian fit for four maxima [intensity calibrated by that of the isotropic liquid using I_{rel} = I(80 °C) / I(115 °C, isotropic liquid)], the distribution function calculated from the two intense peaks which are situated well within the non-shadowed part of the diffraction pattern was used to calculate the order parameter; (b) layer reflections at 80 °C and 106 °C with Gaussian fits; the full width on half maximum for both peaks are 9.9° at 80 °C and 11.6° at 106 °C.

The 1D ^{13}C NMR spectra recorded in the different mesophases, have also been utilized to measure the orientational order parameter of compounds **3** and **4**. For each i^{th} carbon nucleus in the molecule, the chemical shift, δ_{zz}^{i} as obtained from the static ^{1}H-decoupled ^{13}C spectra in the uniaxial LC phases [figure 4.9], represents the average component of the shift tensor along the applied magnetic field. It has been assumed that throughout the mesophases, the rings A and B maintain a nearly parallel orientation with respect to the molecular long axis. The effective order parameter (S) can be approximated by [1, 17, 18]

$$S = \frac{\delta_{zz}^{i}}{\delta_{\zeta\zeta}^{i}} \qquad (4.2)$$

where $\delta_{\zeta\zeta}^{i}$ represents the average anisotropic shift in the molecular frame of reference. The order parameter has been calculated for the carbon atoms in the

para-positions, i.e., 1, 4, 5 and 8. The $\delta_{\zeta\zeta}^{i}$ values have been collected from measured rod-like reference molecules and fitted by their ratios (84.5, 85.75 97.49 and 91.30 ppm for i = 1, 4, 5 and 8 respectively) [1]. An average of these yielded four order parameter values at a particular temperature gives the mean order parameter at this temperature. The temperature dependence of $\langle P_2 \rangle$ as obtained from the NMR measurements in compounds **3** and **4** is shown in figures 4.7(c) and (d). The order increases in all materials within the *N* phase and decreases in the Sm-C_s and Sm-C_a phases.

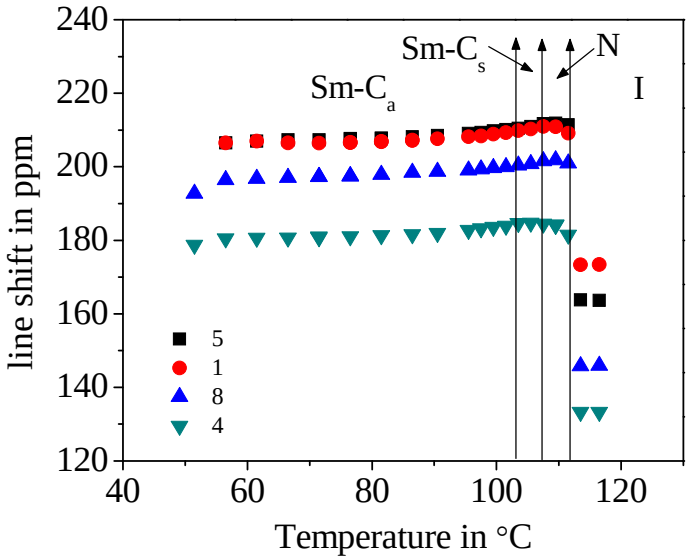

Figure 4.9. Temperature dependence of the line shifts in the ^{13}C NMR spectrum of compound **4**.

It is observed that the order parameter, $\langle P_2 \rangle$ from X-ray diffraction measurements varies quite strongly in the Sm-C_s phase. As shown in figure 4.7(d) such a pronounced temperature dependence of the $\langle P_2 \rangle$ values in the Sm-C_s phase has also been observed in the birefringence measurements. Furthermore, close to the clearing temperature, $\langle P_2 \rangle$ values obtained from the birefringence measurements were always found to be lower than those obtained from the NMR studies. Such a shortcoming is perhaps due to the fact that in NMR measurements one probes the short-range order, which drops slowly on

approaching the nematic-isotropic (*N–I*) transition while in birefringence measurements one investigates the long-range order, which again decreases much rapidly in vicinity of the *N–I* transition.

Similarly to the procedure for deriving the birefringence from measurements of the transmitted intensity, the approach that was used for calculating the order parameters $<P_2>$ from X-ray diffraction measurements was originally developed for a well-aligned nematic phase of calamitic molecules [16]. Here, it is applied to the surface-aligned smectic phases of more or less calamitic (Sm-C_s) and hockey-stick shaped (Sm-C_a) molecules to get a qualitative impression about the changes in the order with temperature. The resulting $<P_2>$ values in the Sm-C_a phase are very large in comparison to those in the Sm-C_s or *N* phase. Again, similar to the birefringence measurements, the orientational order parameter values determined from both the X-ray diffraction and NMR measurements also show only weak temperature dependence in the Sm-C_a phase. The orientational order parameter values obtained from the birefringence and NMR measurements were found to be in well agreement, specifically at the high temperature region. Figure 4.7(d) shows that in the Sm-C_a phase, the $<P_2>$ values obtained from X-ray diffraction measurements are considerably larger than those obtained from both optical birefringence and NMR studies. This apparent contradiction between the two sets of values may be due to the different uncertainties in the three different approaches used. From the X-ray diffraction measurements the $<P_2>$ values have been determined after extracting the azimuthal intensity distribution from the χ–scan [figure 4.8]. However, such intensity distribution may get influenced to some extent by the shadowing of the pattern due to the heating stage and hence, affects the evaluated $<P_2>$ values. The χ–distribution is also influenced by the degree of the alignment of the layers in different regions of the irradiated portion of the sample. Here, a mosaic spread of the layers has to be taken into account [16]. Qualitatively, the alignment in the Sm-C_a phase was found to be slightly improved than that in the Sm-C_s phase as can be seen by

comparing the χ–distribution of the intensity of their layer reflections, which is related to the distribution of the directions of the layer normal [figure 4.8(b)]. Generally speaking, the uncertainties are rather large in case of a surface aligned smectic sample. If it is considered that parts of the sample can gradually reorient during cooling within one phase, even the trend in the change of the orientational order parameters becomes a little uncertain. On the other hand, as mentioned earlier, the tilting of the molecules with respect to the layer normal lowers the value of the orientational order parameter from birefringence measurements. Moreover, the same reason also causes decrease in the $<P_2>$ values in the Sm-C_s phase obtained from the NMR studies. Again, the fact that certain degree of arbitrariness involved in the estimation of the absolute birefringence Δn_0 [equation (4.1)] also imparts a relative shift to the values of the order parameters $<P_2>$, as determined from the birefringence measurements. It may be mentioned that the process of determination of the orientational order parameter from optical and X-ray studies involves taking into consideration the average effect of the contribution from the entire molecule. However, in contrast, an NMR measurement endows the possibility of accessing the local orientational order corresponding to different segments of the molecule.

4.9. Dielectric spectroscopy investigations

The dielectric spectra of compound **5** were taken in the frequency range between 0.1 Hz and 10 MHz. Figure 4.10 shows the real and imaginary part of the complex dielectric function $\varepsilon^*(f) = \varepsilon' - j\varepsilon''$ ($j^2 = -1$) parallel to the director. The measured values perpendicular to the director are illustrated in figure 4.11.

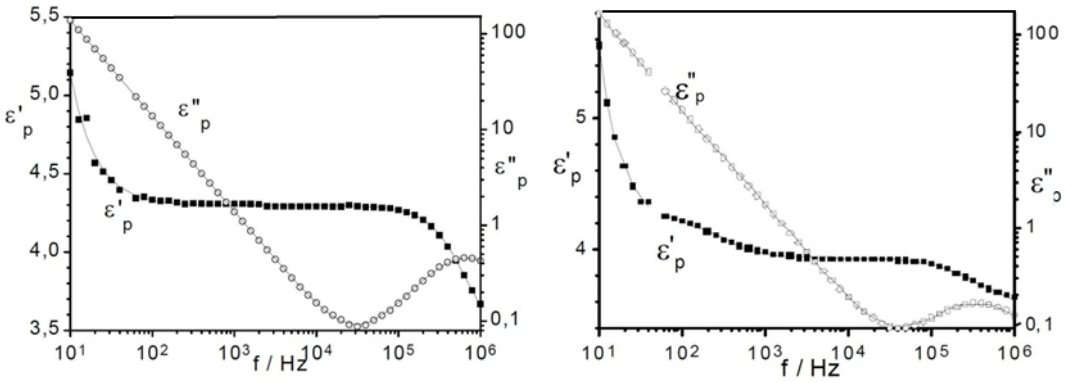

Figure 4.10. The complex dielectric function of compound **5** for the starting orientation parallel to the nematic director, measured in (a) the *N* phase (110 °C) and (b) the Sm-C_s phase (107.5 °C).

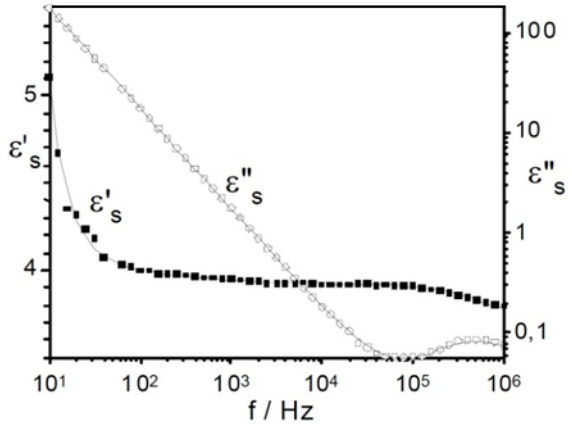

Figure 4.11. The complex dielectric function of compound **5** at 107.7 °C. The director was oriented in the *N* phase perpendicular to the electric field. It is difficult to separate the low frequency absorption at about 200 Hz due to the influence of double layer.

Evaluation of the measured values was carried out using equation (4.3), taking into account two COLE-COLE mechanisms (terms 2 and 3) and the contribution of conductivity in terms 4 and 5 to describe the double layer at low frequencies:

$$\varepsilon^* = \varepsilon_2 + \frac{\varepsilon_0 - \varepsilon_1}{1+(j\omega\tau_1)^{1-\alpha_1}} + \frac{\varepsilon_1 - \varepsilon_2}{1+(j\omega\tau_2)^{1-\alpha_2}} - \frac{jA}{f^M} + \frac{B}{f^N} \qquad (4.3)$$

with ε_i as low, middle and high frequent limiting values of the dielectric constant, $\omega = 2\pi f$ (f = frequency), $\tau_i = 1/2\pi f$ (τ_i = relaxation time), α_i = Cole-

Cole distribution parameter (phenomenological description of the distribution of relaxation times or the superposition of discrete relaxation processes), the conductivity term A as well as M, B and N as further parameters. The conductivity κ calculated according to $\kappa = 2 \cdot A \cdot \pi \cdot \varepsilon_0$ in parallel direction, is shown in figure 4.12.

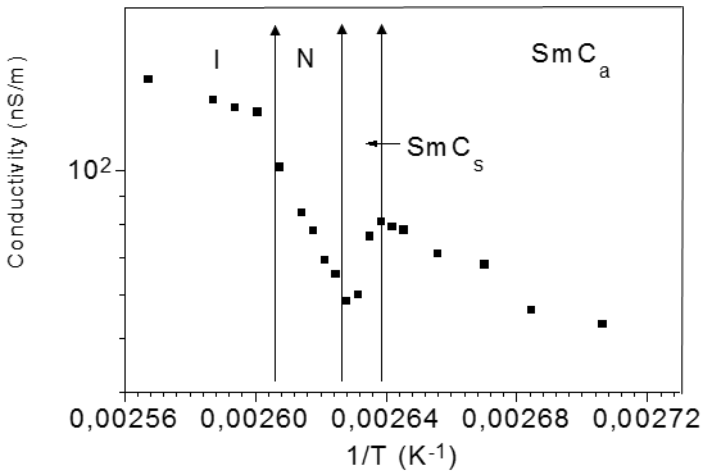

Figure 4.12. Conductivity of compound **5** measured parallel to the director.

The conductivity clearly reflects all the phase transitions. The phase transition Sm-C_s–Sm-C_a is clearly identifiable in the specific conductivity, certainly as a result of the tilt change. To evaluate the limiting values of the dielectric permittivities with the starting orientation of the measuring field parallel to the director by equation (4.3), two relaxation mechanisms with relaxation frequencies at approximately 200Hz and 5 MHz were assumed for the Sm-C phases. In the perpendicular direction only the mechanism at 5 MHz could be detected clearly.

Figure 4.13 shows the limiting values of the dielectric function. At the transition from the isotropic to the nematic state, ε_{P1} increases, indicating a small positive dielectric anisotropy of about 0.35. The low-frequency absorption could neither be observed in the nematic [figure 4.10(a)] nor in the isotropic phase. In both phases only the high-frequency absorption region was visible. The evaluation of the data becomes difficult in the nematic phase because of the influence of standing waves in the measuring cell. For this

reason all values for ε_{P2} given in figure 4.13 as closed triangles and the related relaxation times in figure 4.14 as closed squares show a systematic error in the nematic phase. Nevertheless, it has to be mentioned that this relaxation range exists in the nematic phase too. Relaxation time calculated by equation (4.3) has been illustrated in figure 4.14. Activation energies (54 kJ mol^{-1} for the low frequency mechanism and 92 kJ mol^{-1} for the high frequency mechanism) have also been calculated.

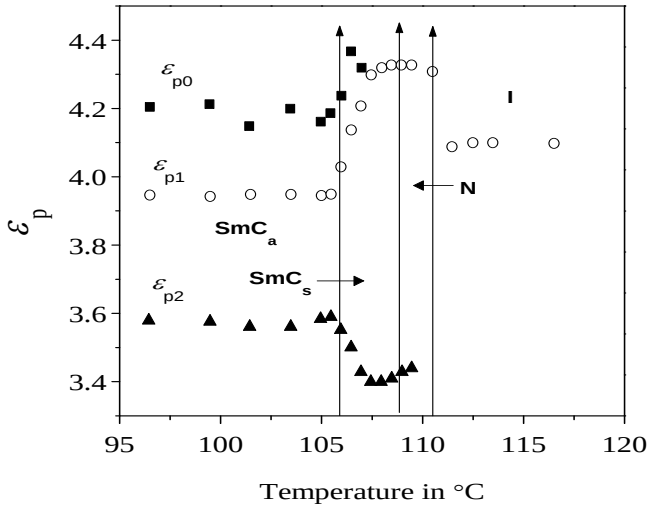

Figure 4.13. Limiting values of the dielectric constant of compound **5** parallel to the director.

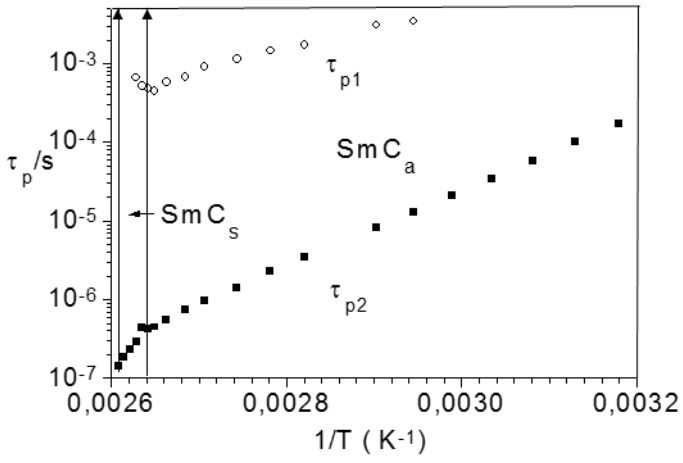

Figure 4.14. Relaxation times of compound **5** measured in the parallel direction.

The relaxation times of the high frequency process agree well with those measured in the parallel direction indicating that it arises from the same mechanism [figures 4.10(b) and 4.11]. The low frequency process could be separated in the perpendicular direction only at high temperatures. This less intensive mechanism is strongly disturbed by the conductivity and the double layer. The relaxation frequencies agree approximately with those found in the parallel direction. For the nematic phase, the low frequency process is not observable. The high frequency relaxation process could be well separated. The dielectric permittivities ε_{P2} and ε_{S2} are larger than 3.5 in the Sm-*C* phase. Thus, there must be at least one further high frequency relaxation process to decrease the dielectric permittivities to about 2.8. From the facts that the relaxation times of the low frequency mechanism are of about 500 Hz and that the associated activation energy is much lower than that of the high frequency mechanism it may be concluded that this process can be compared with the slow dynamics of banana-shaped molecules [19]. It should be noted that in "classical" Sm-*C* phases only one reorientation process in the MHz range with activation energy of about 120 kJ mol^{-1} is usually observed [20]. This process is related to the reorientation of the molecules about the short axes. Also, in this case, the high frequency limit of the dielectric permittivity is more than 3. Assuming that the hockey stick-like molecules form small "soft" ferroelectric clusters the low frequency mechanism can be interpreted as a collective motion of the clusters like that in the phases of banana-shaped molecules [21]. Then the high frequency mechanism should be related to the reorientation of the molecules about the short axes whereas the reorientation around the long molecular axes appearing at higher frequencies was not visible in the present investigated range.

4.10. Electro-optical investigations

Electro-optical measurements were carried out on compound **4** using commercial polyimide coated EHC cells of different thickness. Figure 4.15(a)

shows the fan-shaped texture of the Sm-C_a phase. On applying an electric field the texture nearly remains the same, but the colors clearly change depending on the strength of the field. The textures of the switched states are independent of the polarity of the applied field.

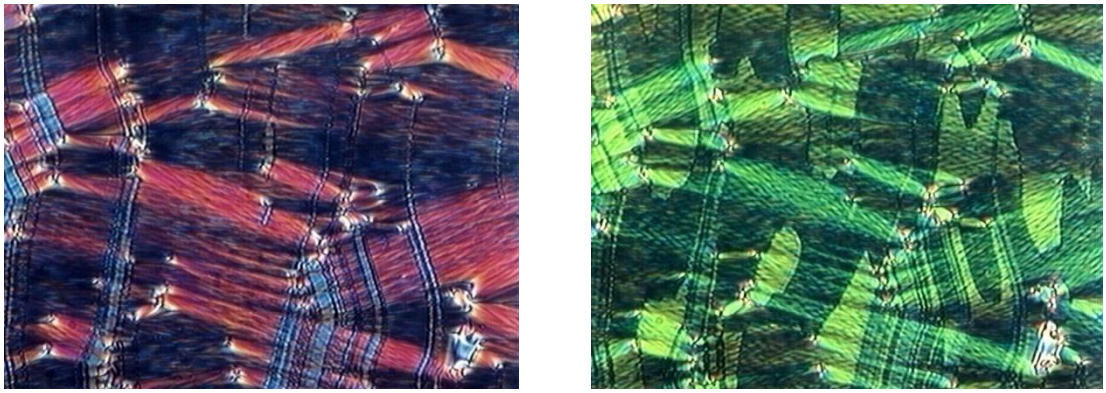

(a) (b)

Figure 4.15. (a) Fan-shaped texture of the Sm-C_a phase without electric field (compound **4**, cell thickness 6 μm, 100 °C); (b) texture after applying a dc field of ±40 V.

The electro-optical behavior was found to be similar in 2 μm EHC cells. It should be noted that only in such very thin cells unusually nice pictures of the Sm-C_s–Sm-C_a phase transition could be observed [figure 4.16, without electric field]. The texture of the Sm-C_s phase of compound **4** at 104 °C is shown in figure 4.16(a). On slow cooling, zig-zag patterns grow [figure 4.16(b)], until the entire area consists of the Sm-C_a phase [figure 4.16(c)]. Decrossing the polarizer by ±15° causes dark and bright domains to appear proving that the tilt of the molecular long axes is opposite in the different domains [figures 4.16(d)–(f)].

Hockey-stick mesogens have a molecular shape that is neither rod-like nor banana-shaped. Therefore, efforts to measure the spontaneous polarization are of great interest. However, the results are not really conclusive. Using a triangular wave voltage (e.g., EHC cell, 6 μm, 10Hz, 320 V_{pp}) a current response with two peaks can be observed in both Sm-*C* phases, which however

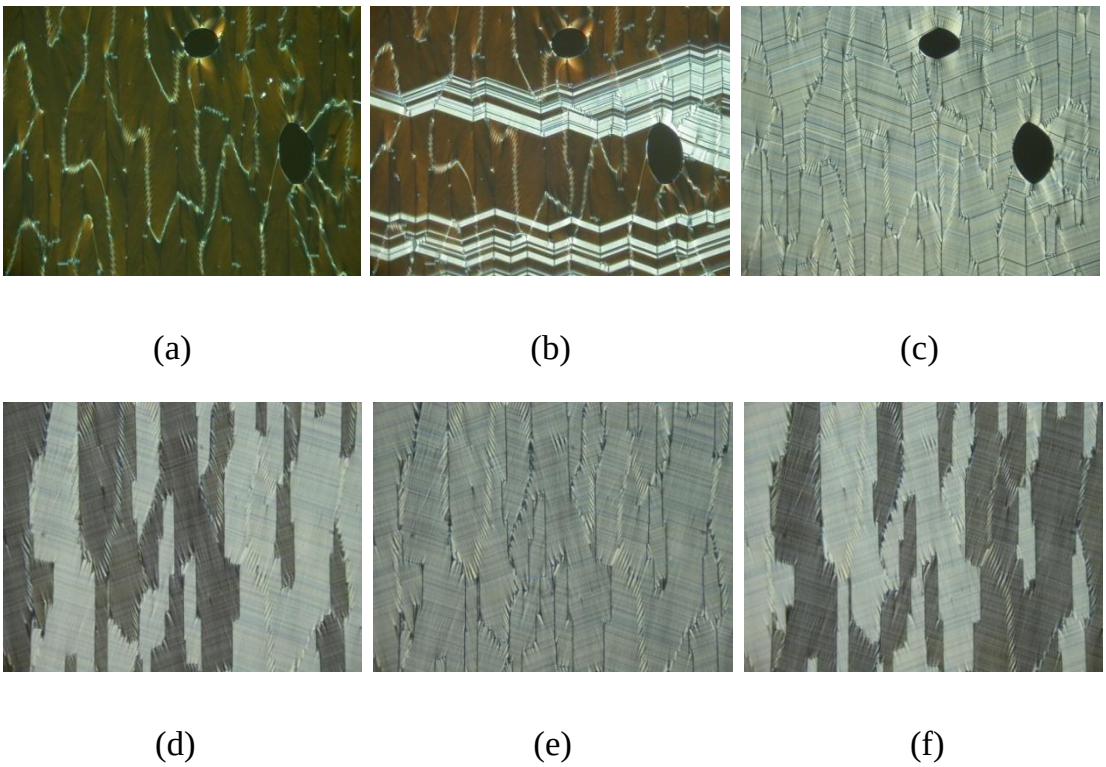

(a) (b) (c)

(d) (e) (f)

Figure 4.16. Compound **4**, 2μm EHC cell polyimide coated, without electric field. (a) Sm-C_s phase at 104 °C; (b) growing of the Sm-C_a phase from the SmC_s phase, 103 °C; (c) Sm-C_a phase at 100 °C. (e) Sm-C_a phase, crossed polarizer at 93 °C; (d) and (f) decrossing the polarizer by +15° or -15°.

does not completely disappear on heating into the isotropic liquid phase. Therefore conductivity measurements did not yield a conclusive polar answer for the compounds under investigation. It can be assumed that the field-induced switching shown in figure 4.15 corresponds to a Freedericksz transition [22] driven by the dielectric anisotropy, because it did not depend on the polarity of the voltage applied.

Yu *et al.* have reported exactly the same behavior and similar problems for other hockey stick-shaped compounds [23, 24]. From electro-optical measurements using mixtures consisting of a hockey stick-shaped compound and a chiral dopant the authors have extrapolated a low spontaneous polarization for the pure non-chiral hockey stick-shaped compound if the concentration of the chiral dopant goes to zero. Furthermore, there is a controversial finding concerning the properties of free-standing films formed

by hockey stick-shaped compounds. Stannarius *et al.* have reported a low, but clearly measurable spontaneous polarization for the high-temperature phase of hockey stick mesogens [2]. The research group of C. C. Huang prepared thin films of definite number between two and ten layers using the same materials. Null transmission ellipsometry and depolarized reflected light microscopy have not given evidence for polar or chiral properties of both smectic phases [3, 25]. Probably, the smectic phases formed by hockey stick mesogens could exhibit a latently polar behavior, which cannot be clearly proved or rejected by the measuring methods used up to date.

4.11. Conclusions

The physical properties of a series of new hockey stick-shaped liquid crystals with a lateral methyl group introduced in the obtuse angle of the molecule, between the *meta*-alkyloxy chain and azomethine connection group have been investigated. It is significant that such a lateral substitution into the molecular core of these mesogens results in the suppression of the Sm-*A* phase and in the introduction of the *N* phase. Steric interactions between the methyl group and the neighboring alkoxy chain in the *meta*-position perhaps induce a more rod-like shape thereby facilitating the formation of the nematic phase at higher temperatures. The *N*–Sm-C_a phase sequence, as observed in **1** and **2,** is also quite remarkable. In addition to the nematic phase, compounds **3**–**5** form two tilted smectic phases – Sm-C_s with synclinic and Sm-C_a with anticlinic molecular arrangement. Together with the other measuring methods used, the optical transmission method conclusively proved the existence of the *N*, Sm-C_s and Sm-C_a phases in these compounds. The two-dimensional X-ray diffraction pattern in the Sm-C_s phase clearly shows the synclinic structure, the pattern in the Sm-C_a phase is caused by an anticlinc arrangement of the molecules in adjacent layers. As observed from previous NMR measurements on closely related hockey stick- shaped compounds, this arrangement of alternating tilt in adjacent layers is accompanied by a pronounced change in the overall shape of

the molecules from a more or less rod-like one in the high temperature Sm-C_s phase to a bent hockey stick-like shape in the lower temperature Sm-C_a phase. The orientational order parameter values determined from the birefringence and NMR measurements agree well with one another and decrease at the Sm-C_s–Sm-C_a transition. However, the $<P_2>$ values determined from X-ray diffraction measurements on compound **4** increase in going from Sm-C_s to Sm-C_a phase and the obtained values are significantly large relative to the other two measuring procedures. This apparent contradiction may be referred to the uncertainties in these methods suffering mainly (but not only) from a differing alignment of the surface-aligned samples in the smectic phases and a differing change in this alignment with temperature for the different experimental settings. Furthermore, a more precise extraction of the X-ray intensity distribution data [I (χ)] and elimination of the background contribution from the same employing other more refined techniques may also help in eliminating such contradicting outcomes.

The dielectric measurements show a low frequency absorption, which is interpreted as signal from ferroelectric clusters in analogy to the polar ferroelectric smectic phases of banana-shaped molecules. It is likely that the clusters formed by hockey stick molecules show stronger fluctuations. Therefore, it may be difficult to detect ferroelectricity by the reversal current methods.

References:

[1] B. Das, S. Grande, W. Weissflog, A. Eremin, M. W. Schröder, G. Pelzl, S. Diele, and H. Kresse, *Liq. Cryst*., **30**, 529 (2003).

[2] R. Stannarius, J. Li, and W. Weissflog, *Phys. Rev Lett*., **90**, 025502 (2003).

[3] X. F. Han, S. T. Wang, A. Cady, Z. Q. Liu, S. Findeisen, W. Weissflog, and C. C. Huang, *Phys. Rev. E*, **68**, 060701 (2003).

[4] G. Sarkar, M. K. Das, R. Paul, B. Das, and W. Weissflog, *Phase Transitions*, **82**, 433 (2009).

[5] E. Enz, S. Findeisen-Tandel, R. Dabrowski, F. Giesselmann, W. Weissflog, U. Baumeister, and J. Lagerwall, *J. Mater. Chem*., **19**, 2950 (2009).

[6] A. Chakraborty, B. Das, M. K. Das, S. Findeisen-Tandel, M. -G. Tamba, U. Baumeister, H. Kresse, and W. Weissflog, *Liq. Cryst.*, **38,** 1085 (2011).

[7] J. Gasowska, R. Dabrowski, W. Drzewinski, K. Kenig, M. Tykarska, and J. Przedmojski, *Mol. Cryst. Liq. Cryst.*, **411**, 231 (2004).

[8] J. Gasowska, R. Dabrowski, M. Filipowich, and J. Przedmojski, *Ferroelectrics*, **343**, 61 (2006).

[9] J. Wu, H. Okamoto, and S. Takenaka, *Chem. Lett*., **30**, 116 (2001).

[10] J. Wu, H. Okamoto, Y. Morita, and S. Takenaka, *Bull. Chem. Soc. Jpn*., **74**, 2437 (2001).

[11] G. Sarkar, B. Das, M. K. Das, U. Baumeister, and W. Weissflog, *Mol. Cryst. Liq. Cryst.*, **540**, 188 (2011).

[12] A. Prasad and M. K. Das, *J. Phys. Conden. Matter*, **22**, 195106 (2010).

[13] M. L. Dark, M. H. Moore, D. K. Shenoy, and R. Shashidhar, *Liq. Cryst.*, **33,** 67 (2006).

[14] I. Haller, *Prog. Solid State Chem.*, **10**, 103 (1975).

[15] B. Bhattacharya, S. Paul, and R. Paul, *Mol. Phys*., **44**, 1391 (1981).

[16] A. K. Leadbetter and E. K. Norris, *Mol. Phys*., **38**, 669 (1979).

[17] H. Sun, M. D. Roth, and B. M. Fung, *Liq. Cryst*., **28**, 1469 (2001).

[18] D. Catalano, L. Chiezzi, V. Domenici, M. Geppi, C. A. Veracini, R. Y. Dong, and K. F. Csorba, *Macromol. Chem. Phys*, **203**, 1594 (2002).

[19] J. Salfetnikova, H. Schmalfuss, H. Nadasi, W. Weissflog, and H. Kresse, *Liq. Cryst*., **27**, 1663 (2000).

[20] H. Kresse, A. Wiegeleben, and D. Demus, *Krist. Tech.*, **15**, 341 (1980).

[21] Z. Vakhovskaya, W. Weissflog, R. Friedemann, and H. Kresse, *Phase Transitions*, **80**, 705 (2007).

[22] G. Pelzl, P. Schiller, and D. Demus, *Liq. Cryst*., **2**, 131 (1987).

[23] F. C. Yu and L. J. Yu, *Chem. Mater*., **18**, 5410 (2006).

[24] F. C. Yu and L. J. Yu, *Liq. Cryst*., **35**, 799 (2008).

[25] S. T. Wang, S. L. Wang, X. F. Han, Z. Q. Liu, S. Findeisen, W. Weissflog, and C. C. Huang, *Liq. Cryst*., **32**, 609 (2005).